Xiaoyun Liu[1]
Shuiqing Zheng[2]
Zheng Jiang[3]
Chen Liang[2]
Rong Wang[2]
Zhe Zhou[3]
Yurong Zhang[2]
Yunqiu Yu[1]

[1]School of Pharmacy, Fudan University, Shanghai, P. R. China
[2]Shanghai Institute of Forensic Science, Shanghai Key Laboratory of Crime Scene Evidence, Shanghai, P. R. China
[3]Thermo Fisher Scientific China Co., Ltd., Shanghai, P. R. China

Received September 24, 2013
Revised January 10, 2014
Accepted January 13, 2014

Research Article

Rapid separation and identification of Strychnos alkaloids metabolites in rats by ultra high performance liquid chromatography with linear ion trap Orbitrap mass spectrometry

An *in vivo* study of Strychnos alkaloids metabolites in rats by ultra high performance liquid chromatography with linear ion trap Orbitrap MS is reported for the first time. Two major Strychnos alkaloids compounds including strychnine and brucine were investigated. To obtain optimal extraction efficiency, samples were pretreated by using an SPE plate. The structures of metabolites and their fragment ions were characterized based on the accurate mass and MS^n data. Forty-seven metabolites were identified in rat urine, of which 25 were reported for the first time. Four new metabolism pathways were proposed on the basis of the identified metabolites. This study provides a practical approach for rapidly identifying complicated metabolites, a methodology that could be widely applied not only in forensic and clinically toxicological relevant cases, but also for the structural characterization of metabolites of other compounds.

Keywords: High-Resolution mass spectrometry / Metabolite identification / Rat urine / Strychnos alkaloids
DOI 10.1002/jssc.201301055

Additional supporting information may be found in the online version of this article at the publisher's web-site

1 Introduction

Strychnos alkaloids (SAs), a class of dihydroindole-type alkaloids, are the predominant active compounds present in the seeds of Strychnos nux-vomica L. The most commonly studied SAs are strychnine (ST) and brucine (BR), which have been widely used as medicine for centuries in tonics for circulatory, respiratory, and digestion disorders. On the other hand, by inhibiting inhibitory neurotransmitters, ST and BR could cause motor disturbance, increase muscle tone and hyperactivity of the senses [1]. High doses of SAs can induce convulsions of the central nervous system and finally death through respiratory paralysis or by cardiac arrest [2]. Thus, the metabolite identification and metabolism study of SAs are extremely important in forensic and clinically toxicological relevant cases [3, 4].

Correspondence: Professor Yunqiu Yu, School of Pharmacy, Fudan University, 826 Zhangheng Road, Shanghai 201203, P. R. China
E-mail: yqyu@shmu.edu.cn
Fax: 0086-21-51980055

Abbreviations: **BR**, brucine; **CMC-Na**, cellulose sodium carboxymethyl; **FWHM**, full width at half maximum; **HRMS**, high-resolution mass spectrometry; **IT**, ion trap; **LTQ**, linear ion trap; **SA**, Strychnos alkaloid; **ST**, strychnine; **UHPLC**, ultra high performance liquid chromatography

The *in vivo* metabolism of ST was investigated from the mid-1960s until the early 1990s, leading to nine metabolites being discovered, such as 2-methoxy-3-hydroxyST and its β-glucuronide conjugate [5], ST *N*-oxide, 2-hydroxyST, ST 21, 22-epoxide, 16-hydroxyST [6], and 22-hydroxyST [7]. In these studies, the metabolites were isolated from biological matrices and then characterized by means of UV and NMR spectroscopy and GC–MS. However, low-abundance metabolites may be neglected using these approaches because of the overlapping signals from high-concentration metabolites.

Since the early 2000s, LC with ion trap (IT) MS has been applied for the identification of SAs metabolites, helping to discover two metabolites: a glucuronide conjugate of ST and demethylation product of BR [8]. LC–IT-MS can provide multistage fragmentations to assist the structural characterization of the SAs metabolites, but its mass accuracy and mass resolution fail to identify traces of metabolites.

High-resolution mass spectrometry (HRMS) offers mass accuracy $\leq$5 ppm and high resolution greater than 10 000 full width at half maximum (FWHM), which is powerful in the analysis of unknown sample from a complicated

*Additional corresponding author: Yurong Zhang,
E-mail: yrzhang803@163.com

Colour Online: See the article online to view Figs. 1 and 5 in colour.

matrix [9–11], thus it has become ubiquitous in the field of metabolites identification [12–14]. 31 metabolites of SAs *in vitro* were identified in an study with rat microsomes by LC–IT-TOF-MS [15]. However, few experiments involving *in vivo* biotransformation have been done through HRMS so far, although *in vivo* studies represent more realistic picture about the metabolism.

In recent years, LC coupled with hybrid linear ion-trap/Orbitrap (linear ion trap [LTQ]-Orbitrap) MS has proven to be a powerful and reliable analytical tool for identifying drug metabolites generated both *in vivo* and *in vitro* [16–18]. LTQ-Orbitrap XL MS is capable of providing high mass resolution (>100 000 FWHM) and performing exact mass MS^n analysis (<3 ppm), increasing confidence in the identification of metabolites of similar accurate mass [19–22].

In our study, ultra high performance liquid chromatography (UHPLC) with LTQ-Orbitrap-MS was first applied to the *in vivo* metabolites identification of ST and BR in rat urine. Metabolites in rat urine were identified and their structures were proposed based on the accurate mass and MS^n mass spectrum data. Possible metabolism pathways in rats were proposed based on the metabolites, which supplemented the reported metabolism characteristics of SAs in rats both *in vivo* and *in vitro*.

2 Materials and methods

2.1 Chemicals and materials

The reference standards, ST and BR were supplied from the National Institute for the Control of Pharmaceutical and Biological Products of China (Beijing, China). ST *N*-oxide and BR *N*-oxide (Purity >99.1% by HPLC) were kindly provided by Professor Pan Yang (Nanjing University of Traditional Chinese medicine). HPLC-grade methanol and acetonitrile were purchased from Merck (Darmstadt, Germany). HPLC-grade ammonium formate and formic acid were purchased from GNW Technologies (Germany). Ultra-pure water was generated by an ELGA Lab water PURELAB Ultra system. Analytical grade hydrochloride, hydrochloric acid, chloroform and isopropanol were purchased from Shanghai Lingfeng Chemical Reagent (Shanghai, China). Cellulose sodium carboxymethyl (CMC-Na) was purchased from Guoyao Chemical (Shanghai, China). An Oasis MCX μElution Plate (30 μm) was obtained from Waters (Milford, MA, USA).

2.2 Animals and Samples collection

Male Sprague–Dawley rats (200–260 g) were supplied by the Shanghai Institute of Pharmaceutical Industry. Rats were fasted for 12 h before drug administration and for an additional 4 h after dosing. Water was freely available for rats during experiments. In order to collect urine sample, the rats ($n = 6$) were kept in individual metabolic cages. Six rats were then randomly divided into two groups, one group ($n = 3$) was orally administered a single dose of ST (5 mg/kg, adding 0.5% CMC-Na), and the other was orally administered a single dose of BR (10 mg/kg, adding 0.5% CMC-Na). All studies on animals were performed with the approval of the Institutional Authority for Laboratory Animal Care. Urine samples were collected 0∼6 h after oral administration of ST and BR, respectively. All samples were immediately frozen at −20°C until analysis.

2.3 Sample pretreatment

A special SPE was applied to rat urine samples by using an Oasis MCX μElution 96-Well Plate (30 μm; Waters, USA) to separate and enrich the metabolites from the urine samples. The plate was first conditioned with 200 μL of methanol and then 200 μL of purified water. Two hundred microliters of urine was combined with 100 μL of 0.05 mol/L HCl, then vortex-mixed for 30 s and loaded into the individual well. The cartridge in the well was washed with 300 μL of 2% aqueous formic acid and 300 μL of methanol and finally eluted with 50 μL of 5% ammonium in methanol. The eluent was finally mixed with 50 μL of 6% aqueous formic acid and 5 μL of this sample was injected into the UHPLC–LTQ-Orbitrap-MS system. This pretreatment method is fast, high-throughput, and reproducible, it resulted in higher recovery and allowed sample small volumes to be analyzed.

2.4 Chromatographic separation and UHPLC–MS conditions

An Accela HPLC system (Thermo Fisher Scientific) was equipped with a built-in vacuum degasser, an autosampler and a quaternary pump. The separation was performed on a Hypersil Gold C_{18} column (100 × 2.1mm, 1.9 μm) and the temperature was set at 30°C. The mobile phase was composed of solvent A (2 mM ammonium formate and 0.05% formic acid in water) and solvent B (2 mM ammonium formate and 0.05% formic acid in acetonitrile). Gradient elution with the flow rate of 0.2 mL/min was linearly programmed as follows: 10% B (0–1 min), 10–20% B (1–11 min), 20–70% B (11–18 min), 70–100% B (18–20 min), then back to initial 10% B (20–23 min) and held for 5 min for re-equilibration. The injection volume was 5 μL.

Metabolites were analyzed by a Finnigan LTQ-Orbitrap XL instrument with an ESI source (Thermo Electron, Bremen, Germany). The MS parameters were optimized by direct infusion of 1.0 μg/mL BR in methanol. Nitrogen was used as both the sheath gas (35 units) and auxiliary gas (8 units). Values of tube lens and capillary voltages were set to 120 and 39 V, respectively. The ionization voltage was 4.0 kV, and the capillary temperature was set at 275°C. The scan event cycle used a full scan mass spectrum with a resolution setting of 30 000, a data-dependent MS^2 event including a predicted metabolites precursor list with a resolution setting of 15 000 and a corresponding data-dependent MS^3 event with a

resolution setting of 7500. The most abundant ion was selected to trigger data-dependent scans if there was no match with the precursor list or the most intense ion. Collision-induced dissociation was conducted with an isolation width of 2 Da, normalized collision energy was 35%, and activation time was 30 ms.

2.5 Data processing

MS data processing was carried out using the QualBrowser of Xcalibur 2.1 Software (Thermo Fisher Scientific), including extracted ion chromatograms, calculation of elemental compositions using potential metabolite ions with 5 ppm mass tolerance. MetWorks 1.3 Software (Thermo Fisher Scientific) was set to automatically identify metabolites by comparing the sample with the control. Structures of the detected metabolites were characterized based on their MS shifts from the parent drug, their fragmentation patterns and elemental compositions. Possible metabolic pathways of ST and BR of Phase I and Phase II were defined individually in the modification manager. In addition, Mass Frontier 6.0 Software (Thermo Fisher Scientific) was used in aiding MS^n spectral interpretation of metabolites.

3 Results and discussion

3.1 Optimum conditions for UHPLC–MS analysis

The conditions of mass spectra analysis for ST and BR were optimized in both positive and negative modes. Our results found that the positive ion mode produced more product ions than the negative ion mode. Therefore, the positive mode was selected for the following ESI analysis. We also found that the addition of formic acid into the mobile phase enhanced signal intensity of metabolites, which could aid the identification of unknown metabolites. Different concentrations of formic acid (0.01, 0.05, 0.1% v/v) and ammonium formate (1, 2 and 5 mM) were tested in order to identify the mobile phase that may produce the highest sensitivity. Results showed peak intensity increased dramatically when 0.05% formic acid and 2 mM ammonium formate were added into the mobile phase. Therefore, a mobile phase of 0.05% formic acid and 2 mM ammonium formate in both water and acetonitrile was selected for LC–ESI-MS analysis.

3.2 Tentative Identification of SAs metabolites

ST, BR, and their metabolites in rat urine were identified with the aid of MetWorks 1.3, as shown in Fig. 1. The observed and calculated masses were < 3 ppm, providing high confidence in the proposed elemental composition of the metabolites (Table 1) . No significant qualitative differences were observed in the metabolite profiles of SAs among different rats.

ST (M_0) was eluted at a retention time of 9.35 min and showed as a protonated molecule at m/z 335.17567. The MS^2 analysis of the $[M + H]^+$ ion showed a predominant fragment ion at m/z 264.10220 and several fragment ions of significant abundance at m/z 307.14456, 290.11792, 272.10733, 234.09154, 222.09158, 184.07581, and 156.08076. To obtain further information on the peak at m/z 264.10220, the MS^3 spectrum (Fig. 2A) was acquired. Based on the data and the aid of Mass Frontier 6.0, the possible fragmentation pathways of ST were proposed (Fig. 2B). The peak at m/z 307.14456 could be formed by partial loss of nitrogen bridge (loss of C_2H_4 at C_{17}–C_{18}) and cleavage at C_7 and C_{17}, N_{19}, and C_{18}, and hydrogen transfer from C_8 to N_{19}. Moreover, it could further form the base peak at m/z 264.10220, through a neutral loss of C_2H_5N (C_{15}–C_{16}–N_{19}) and rearrangement of the six-membered ring located at C_7, C_8, C_{13}, C_{14}, C_{15}, and C_{16}. The peak at m/z 264.10220 could lose part of the seven-membered ring to form fragment ions at m/z 222.09158 and 184.07581, and further produce a neutral loss of CO to form fragment ions at m/z 194.09633 and 156.08076. These product ions were used as references to interpret the product ions of BR and the metabolites.

BR (M_0') showed a very similar fragmentation pattern (Supporting Information Fig. S1A) with ST except with two additional methoxyl groups. Therefore, most product ions found in ST were also detected in BR with a mass shift of 60 Da. Nevertheless, the fragment ion at m/z 263.09442 was uniquely observed in the MS^2 spectrum of BR. The mass difference between fragment ions at m/z 294.11295 and 263.09442 was 31 (a CH_3O. radical), which could be explained by the presence of methoxyl groups connected to a benzene ring. The proposed fragmentation mechanism of BR was similar to that of ST (Supporting Information Fig. S1B).

3.2.1 Identification of ST metabolites

Twenty-six metabolites of ST, including 22 phase I and 4 phase II metabolites, were identified in rat urine. The possible structural elucidation was as follows.

M_1–M_6 were observed as average $[M + H]^+$ at m/z 351.17074, suggesting that they were isomers of hydroxylation or oxidation metabolites of ST (Fig. 3). M_1 produced product ions at m/z 323.13653, 280.09726, 250.06662, 238.08658, and 200.07088, which were all 16 higher than the corresponding product ions of ST, suggesting that the hydroxylation reaction might be on the benzene ring. According to Mass Frontier, predominant fragment ion at m/z 280.09726 can be better explained when the reaction sites narrowed down to C2 or C3 [6]. M_1, thus was proposed to be 2-hydroxyST or 3-hydroxyST.

The MS^2 fragmentation patterns of M_2 were very similar to those of ST, such as m/z 272.10745, 238.08656, 222.09154, and 184.07591, which suggests that the basic skeleton of ST remain unchanged. A mass difference of 2 Da in some other fragments (m/z 290.11801 and 288.10239, 264.10236, and 262.12305) could be explained by the C = C bond formed by H_2O elimination at the seven-membered

Table 1. LC–MS^2 data of ST and BR metabolites in rat urine

Metabolite	Observed $[M+H]^+$ (m/z)	Elemental composition $[M+H]^+$	Calculated $[M+H]^+$ (m/z)	Error (ppm)	R.T. (time)	MS^2 product ions	Identification	Reference
M_0	335.17567	$C_{21}H_{23}O_2N_2$	335.17540	0.79	9.35	184,194,222,234,**264**,290,307	ST	
M_1	351.17050	$C_{21}H_{23}O_3N_2$	351.17032	0.515	5.83	238,250,278,**280**,288,306,323, 333	2-HydroxyST or 3-HydroxyST	[6]
M_2	351.17078	$C_{21}H_{23}O_3N_2$	351.17032	1.31	6.57	200,222, 238,262,272,**280**,290,322,333	ST 21,22-epoxide	[23]
M_3	351.17068	$C_{21}H_{23}O_3N_2$	351.17032	1.03	7.55	184,220,236,248,260,278,296,307,315.,**333**	22-HydroxyST	[7]
M_4	351.17072	$C_{21}H_{23}O_3N_2$	351.17032	1.14	9.24	238,264,278,290,307,**333**	16-HydroxyST	[15]
M_5	351.17100	$C_{21}H_{23}O_3N_2$	351.17032	1.94	10.86	306, **334**	ST N-oxide	[6]
M_6	351.17075	$C_{21}H_{23}O_3N_2$	351.17032	1.13	11.37	184,220,238,250,**280**,288,319,323,334	HydroxyST	
M_7	353.18604	$C_{21}H_{25}O_3N_2$	353.18597	0.198	7.43	156,**184**,222,234,248,272,290,307,324,335	21-Hydro-22-hydroxy or 22-hydro-21-hydroxyST	[15]
M_8	369.18097	$C_{21}H_{25}O_4N_2$	369.18088	0.234	6.32	184,212,220,280,327,333,**351**	21,22-Dihygroxy-22-hydroST	[24]
M_9	369.18100	$C_{21}H_{25}O_4N_2$	369.18088	0.315	7.22	184,212,333,**351**	21,22-Dihygroxy-22-hydroST	[24]
M_{10}	369.18103	$C_{21}H_{25}O_4N_2$	369.18088	0.396	8.12	**351**	Dihydroxy-22-hydroST	
M_{11}	365.18649	$C_{22}H_{25}O_3N_2$	365.18597	1.42	10.81	220,234,248,262,272,290,294,**305**,333,347	MethoxyST	
M_{12}	365.18634	$C_{22}H_{25}O_3N_2$	365.18597	1.02	11.46	214,252,264,**294**,302,320,337	2-MethoxyST or 3-methoxyST	[15]
M_{13}	365.18646	$C_{22}H_{25}O_3N_2$	365.18597	1.34	11.87	220,234,248,262,272,290,294,**305**,333,347	MethoxyST	
M_{14}	367.16528	$C_{21}H_{23}O_4N_2$	367.16523	0.136	3.59	200,226,238,250,278,304,**321**,338,349	DihydroxyST	
M_{15}	367.16537	$C_{21}H_{23}O_4N_2$	367.16523	0.381	4.51	200,236,253,278,**296**,322,339,349	2,3-DihydroxyST	
M_{16}	367.16531	$C_{21}H_{23}O_4N_2$	367.16523	0.218	5.10	200,226,260,276,304,321,**349**	DihydroxyST	
M_{17}	367.16537	$C_{21}H_{23}O_4N_2$	367.16523	0.381	6.09	184,220,236,280,307,331,**349**	DihydroxyST	
M_{18}	367.16534	$C_{21}H_{23}O_4N_2$	367.16523	0.300	7.15	196,220,238,258,276,304,322,**349**	DihydroxyST	
M_{19}	367.16541	$C_{21}H_{23}O_4N_2$	367.16523	0.490	7.83	184,220,238,278,305,321,**349**	DihydroxyST	
M_{20}	367.16544	$C_{21}H_{23}O_4N_2$	367.16523	0.572	8.74	184,220,236,278,294,335,**350**	21,22-Epoxide-N-oxide ST	[15]
M_{21}	333.16028	$C_{21}H_{21}O_2N_2$	333.15975	1.59	9.21	220,264,**278**,290,315	11,12-DehydroST	[24]
M_{22}	333.16049	$C_{21}H_{21}O_2N_2$	333.15975	2.22	15.90	—	DehydroST	
M_{23}	527.20251	$C_{27}H_{31}O_9N_2$	527.20241	0.19	2.60	**351**	Glu conjugate of M_1	
M_{24}	527.20239	$C_{27}H_{31}O_9N_2$	527.20241	0.04	3.62	**351**	Glu conjugate of M_2	
M_{25}	527.20251	$C_{27}H_{31}O_9N_2$	527.20241	0.19	5.02	**351**	Glu conjugate of M_3	
M_{26}	511.20755	$C_{27}H_{31}O_8N_2$	511.20749	0.12	7.38	—	Glu conjugate of ST	[8]
M_0'	395.19702	$C_{23}H_{27}O_4N_2$	395.19653	1.24	10.01	244,282,294,**324**,332,350,367,380	BR	
M_1'	381.18115	$C_{22}H_{25}O_4N_2$	381.18088	0.71	6.60	268,**310**,311,336,353,366	Demethylation-BR	[5]
M_2'	381.18118	$C_{22}H_{25}O_4N_2$	381.18088	0.78	7.94	268, **310**,311,336,353	Demethylation-BR	[5]
M_3'	411.19186	$C_{23}H_{27}O_5N_2$	411.19145	0.997	7.25	280,282,294,322,340,**365**,366,383,393	22-HydroxyBR	[15]
M_4'	411.19189	$C_{23}H_{27}O_5N_2$	411.19145	1.07	8.24	229,244,**280**,298,308,326,338,366,383,396	HydroxylBR	[15]
M_5'	411.19177	$C_{23}H_{27}O_5N_2$	411.19145	0.778	8.64	229,**244**,280,304,320,348,365,396	12-HydroxyBR	[15]
M_6'	411.19186	$C_{23}H_{27}O_5N_2$	411.19145	0.997	9.81	244,280,298,324,320,350, 367,**393**	16-HydroxyBR	[15]
M_7'	411.19180	$C_{23}H_{27}O_5N_2$	411.19145	0.851	11.16	379,393,**394**	BR N-oxide	[6]

Table 1. Continued

Metabolite	Observed $[M+H]^+$ (*m/z*)	Elemental composition $[M+H]^+$	Calculated $[M+H]^+$ (*m/z*)	Error (ppm)	R.T. (time)	MS^2 product ions	Identification	Reference
M_8'	427.18658	$C_{23}H_{27}O_6N_2$	427.18637	0.49	6.81	280,325,**363**,383,395,399,409	Dihydroxyl-BR	
M_9'	427.18643	$C_{23}H_{27}O_6N_2$	427.18637	0.14	7.18	244,280,324,340,354,381,399,**409**,413	Dihydroxyl-BR	
M_{10}'	427.18692	$C_{23}H_{27}O_6N_2$	427.18637	1.28	7.45	244,280,298,320,337,364,**382**,399,409,412	Dihydroxyl-BR	
M_{11}'	427.18655	$C_{23}H_{27}O_6N_2$	427.18637	0.42	8.92	244,280,297,309,338,365,381,399,**409**	Dihydroxyl-BR	
M_{12}'	427.18671	$C_{23}H_{27}O_6N_2$	427.18637	0.8	11.47	282,298,322,336,356,364,**367**,381,395,409	Dihydroxyl-BR	
M_{13}'	429.20218	$C_{23}H_{29}O_6N_2$	429.20201	0.396	6.94	244,272,280,282,340,365,393,401,**411**	21,22-Dihygroxy-22-hydroBR	
M_{14}'	429.20261	$C_{23}H_{29}O_6N_2$	429.20201	1.4	7.49	244,272,280,282,340,365,384,393,**411**	21,22-Dihygroxy-22-hydroBR	
M_{15}'	429.20288	$C_{23}H_{29}O_6N_2$	429.20201	2.02	8.15	244,280,306,323,342,349,367, 393,401,**411**	Dihydroxy-22-hydroBR	
M_{16}'	557.21374	$C_{28}H_{33}O_{10}N_2$	557.21297	1.38	1.36	**381**	Glucuronide conjugate of Demethylation-BR	[5]
M_{17}'	557.21344	$C_{28}H_{33}O_{10}N_2$	557.21297	0.84	2.59	**381**	Glucuronide conjugate of Demethylation-BR	[5]
M_{18}'	557.21295	$C_{28}H_{33}O_{10}N_2$	557.21297	−0.04	5.32	**381**	Glucuronide conjugate of Demethylation-BR	[5]
M_{19}'	571.22876	$C_{29}H_{35}O_{10}N_2$	571.22862	0.245	6.32	310,336,353,**381**,382,395	Glucuronide conjugate of BR	
M_{20}'	571.22882	$C_{29}H_{35}O_{10}N_2$	571.22862	0.35	9.29	310,336,353,**381**,382,393	Glucuronide conjugate of BR	
M_{21}'	571.22235	$C_{29}H_{35}O_{10}N_2$	571.22862	2.96	14.21	318,351,387,**393**	Glucuronide conjugate of BR	

Base peaks were marked in bold font.

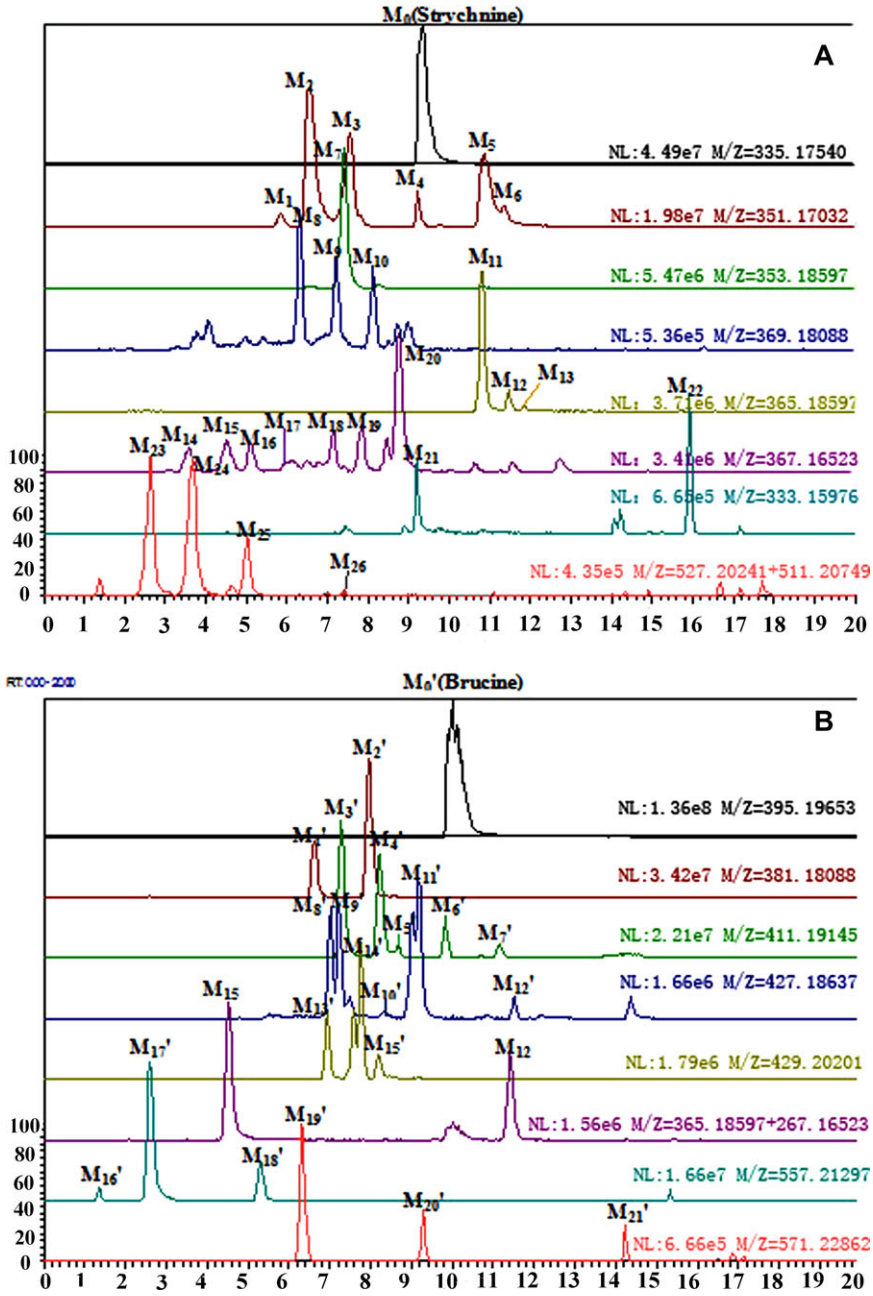

Figure 1. Extracted ion chromatograms of metabolites of ST and BR in male rat urine. BR shared two common phase-I metabolites, M_{12} and M_{15}, with ST.

ring, indicating that the double bond at $C_{21–22}$ was epoxidized. Therefore, M_2 was proposed to be ST 21, 22-epoxide [23]. M_3 produced similar product ions to M_2 and was proposed to be structurally similar to M_2. Characteristic product ions at *m/z* 307.14471, 272.10751, 220.07603, and 184.07593 suggested that the basic skeleton remain unchanged, and the hydroxylation reaction might be on the seven-membered ring. Since its fragmentation pattern can be reasonably explained hydroxylation at C_{22}, M_2 was proposed as 22-hydroxyST [7].

M_4 gave rise to product ions at *m/z* 307.14490, 290.11810, 264.10251, 234.09175, and 184.07565, indicating that the oxidation did not occur at any carbon among $C_{1–14}$ or $C_{21–23}$ of the basic skeleton. The predominant peak at *m/z* 333.16023 (loss of H_2O) and characteristic fragment ion at *m/z* 278.11826 (cleavage between C_{20} and C_{21}, C_{16} and N_{19}, C_7 and C_{17}) suggested that hydroxylation site could most likely to be C_{16}. M_4 was thus proposed as 16-hydroxyST [15].

The predominant peak of M_5 at *m/z* 334.16809 (loss of .OH) indicated the instability of the oxygen atom and suggested that the nitrogen atom on the nitrogen bridge might be oxidized. An authentic standard of ST *N*-oxide was used to match retention time, accurate mass, and tandem mass spectrum. Thus, M_5 was confirmed as ST *N*-oxide [6]. M_6 had similar product ions to M_5. However, we could not characterize the exact sites of hydroxylation.

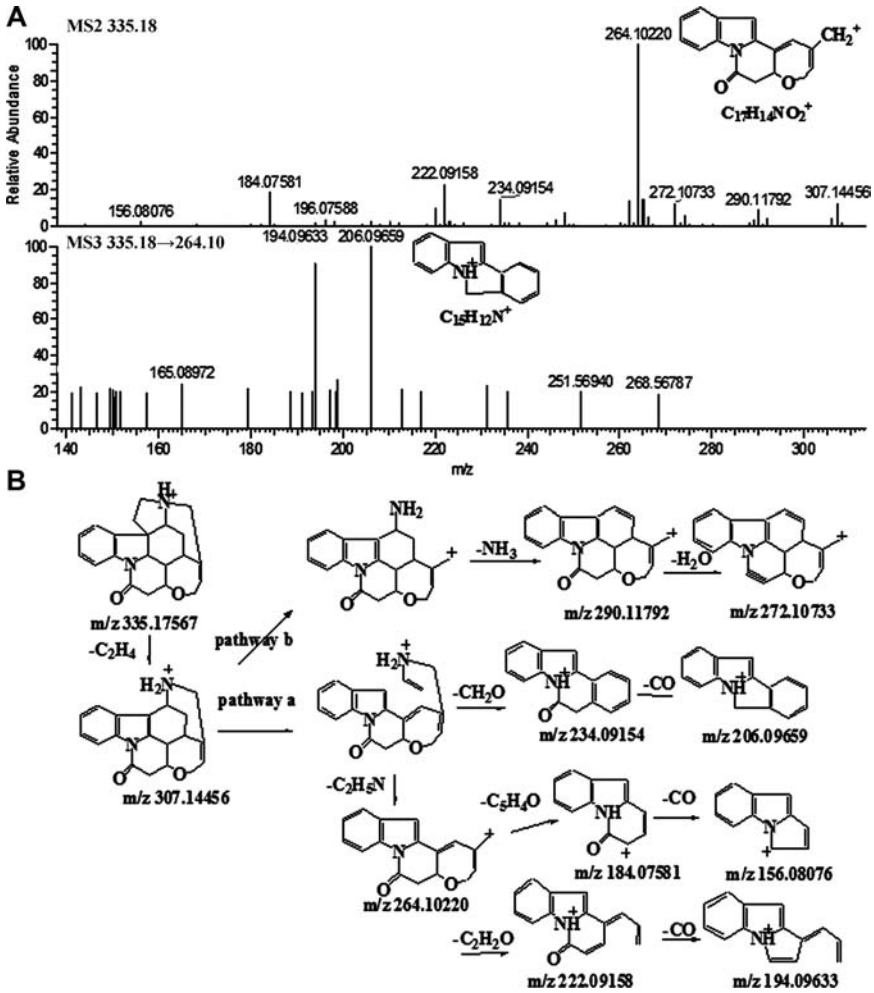

Figure 2. Accurate MS^2 spectrum and MS^3 spectrum (A), proposed fragmentation mechanism of ST (B).

Metabolite M_7 showed the $[M+H]^+$ at m/z 353.18604 and was preliminarily proposed to be the hydrolysis product of ST. The MS^2 fragment ions of M_7 at m/z 222.09186 and 184.07607 (Supporting Information Fig. S2) indicated an unchanged lactam ring and so hydrolysis could not occur on the amide bond. Other low-abundance product ions were mostly formed by the cleavage of the C_{20-21} bond, and thus confirmed the hydrolysis site to the C_{21-22} double bond. Therefore, M_7 was proposed as 21-hydro-22-hydroxyST [15] or 22-hydro-21-hydroxyST.

The average $[M + H]^+$ of M_8–M_{10} at m/z 369.18097 was 34 higher than ST, indicating that they were hydrolysis–hydroxylation products of ST. The predominant fragment ion at m/z 351.17072 (loss of H_2O) suggested the presence of a hydroxyl group. M_8 and M_9 had nearly the same accurate mass and tandem mass spectrum, demonstrating that they had very similar structures. We tried different reaction sites with Mass Frontier, and found that the hydrogenation products of M_7 can reasonably explain product ions of them two, which coincided exactly with 21,22-dihygroxy-22-hydroST described in the literature [24]. Thus, M_8 and M_9 were proposed as isomers of 21,22-dihygroxy-22-hydroST. The MS^3 spectrum of M_{10} (Supporting Information Fig. S3) was similar with the MS^2 spectrum of M_2 (Fig. 3), indicating the existence of C_{22}-hydroxy. As it is hard to characterize the other hydrogenation site, M_{10} was proposed as dihydroxy-22-hydroST.

M_{11}–M_{13} showed average $[M + H]^+$ at m/z 365.18643, which are 30 higher than ST, suggesting that methoxylation occurred in this metabolic process. The characteristic MS^2 fragment ions of M_{12} were at m/z 294.11285, 264.10220, 252.10219, and 214.08646 (Supporting Information Fig. S4), 30 higher than those of ST. M_{12} was also detected as a demethoxylation metabolite of BR, limiting the reaction site to C_2 or C_3. Thus, M_{12} was proposed as 2-methoxyST (β-colubrine) or 3-methoxyST (α-colubrine) [15]. The MS^2 spectrum of M_{11} and M_{13} were alike and, therefore, they were likely to be isomers of similar structures. However, the exact reaction site could not be confirmed. Metabolites M_{14}–M_{20} showed average $[M + H]^+$ at m/z 367.16536, 32 higher than ST, which suggested that they were sequentially oxidized or hydroxylated products of ST. M_{15} showed a characteristic fragment ion (Supporting Information Fig. S4) at m/z 296.03354 and several product ions at m/z 339.25055, 278.18585, 254.14338, which were 32 higher than ST, suggesting the presence of two hydroxyl groups on the benzene ring. M_{15} was also detected as a sequential demethylated

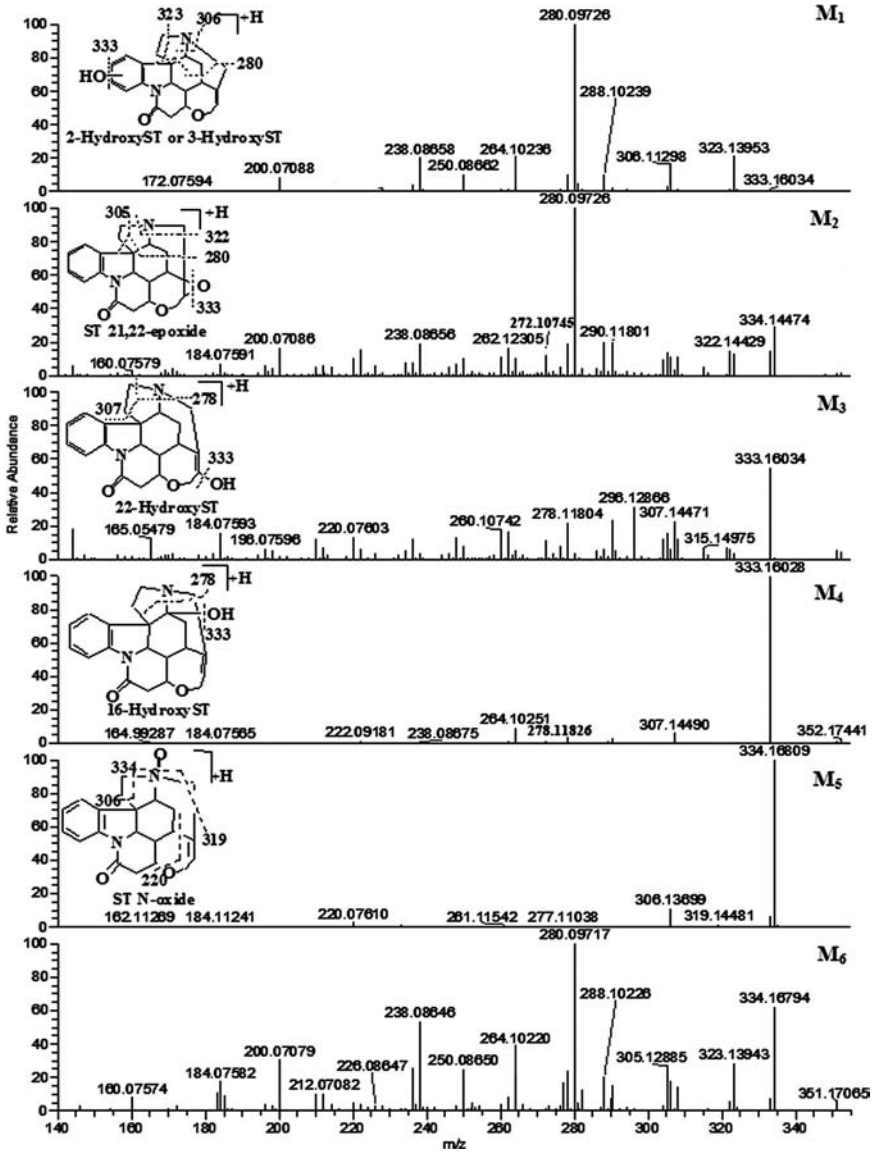

Figure 3. Accurate MS^2 spectra of M_1–M_5. The numbers in brackets indicate the mass-to-charge ratio of the corresponding fragments. The proposed fragmentation mechanism is also listed.

metabolite of BR, which narrowed the reaction sites to C_2 and C_3. Thus M_{15} was proposed as 2,3-dihydroxyST. As for metabolites M_{16}–M_{19}, the MS^2 spectra all exhibited identical base peaks at m/z 349.20554, suggesting that hydroxylation took place on the carbon of the basic skeleton, but the site could not be exactly determined. M_{20} had a base peak at m/z 350.22293 (loss of .OH) in Supporting Information Fig. S4, which was identical to M_5. Low abundance product ions were observed at m/z 335.17554, 321.22383, and 294.11179, corresponding to the cleavage of the C_{20-21} bond. This gave support to the presence of a 21,22-epoxide substitution. Therefore, M_{20} was proposed as 21,22-epoxide-*N*-oxideST [15]. Product ions of M_{14} were detected at a low level and thus no structural assignment could be suggested.

M_{21} and M_{22} showed average $[M + H]^+$ at m/z 333.16039, 2 less than ST, indicating that they were dehydrogenation products of ST. The predominant peak of M_{21} (Supporting Information Fig. S5) at m/z 278.11783 (cleavage between C_{20} and C_{21}, C_{16} and N_{19}, C_7 and C_{17}) and characteristic fragment ion at m/z 264.10226 and 290.11795 (similar with ST) suggested that the reaction occurred on the basic skeleton (C_{1-14} or C_{21-23}). The fragment ion at m/z 315.14984 (loss of H_2O) suggested the possible existence of a keto-enol tautomer at C_{10}–C_{12} [24], which narrows the dehydrogenation sites down to C_{11} and C_{12}. Thus, M_{21} was identified as 11, 12-dehydroST. However, M_{22} could not be further studied by MS^n owing to its too low concentration and thus no exact structural assignment could be suggested.

3.2.1.1 Phase II metabolites of ST

M_{23}–M_{25} showed an average $[M+H]^+$ at m/z 527.20247, 192 more than ST, suggesting that hydroxylation–glucuronidation occurred. The base peak at m/z 351.17075

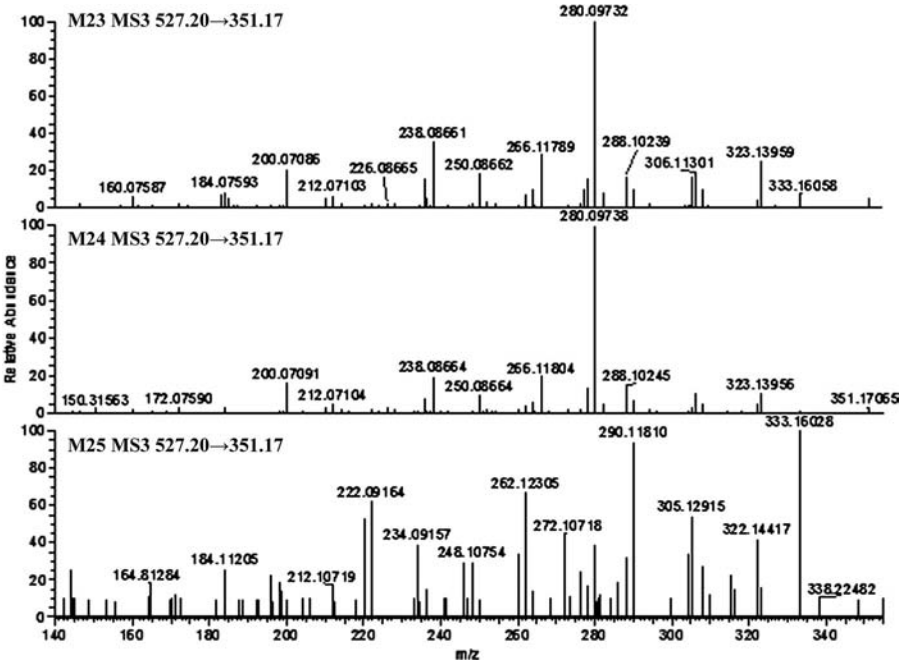

Figure 4. Accurate MS^3spectra of M_{23}–M_{25}.

Table 2. Metabolism pathways differences between the *in vivo* rat model and *in vitro* one

Metabolism pathways	ST		BR	
	In Vivo	*In Vitro*	*In Vivo*	*In Vitro*
Hydroxylation	Y	Y	Y	Y
N–Oxidation	Y	Y	Y	Y
Hydrolysis	Y	Y		
Hydroxylation–hydrolysis	Y	N	Y*	N
Sequential Oxidation	Y	Y	Y	Y
Dehydrogenation	Y	Y		
Methylation–oxidation	Y	Y		
Demethylation			Y	Y
Sequential demethylation			Y*	N
Demethoxylation			Y	Y
Glucuronidation	Y	N	Y*	Y
Hydroxylation–glucuronidation	Y*	N		
Demethylation–glucuronidation			Y	N

Metabolism pathways marked with * were reported for the first time.

(loss of $C_6H_8O_6$) proved them to be glucuronide conjugate of hydroxyl-ST. The corresponding MS^3 spectrum of M_{23}, M_{24}, and M_{25} (Fig. 4) were observed to be similar with the MS^2 spectrum of M_1, M_2, and M_3 (Fig. 3) and thus they were identified to be the glucuronide conjugate of M_1, M_2 and M_3, respectively. The $[M + H]^+$ of M_{26} at m/z 511.20755 was 176 higher than ST, indicating that M_{26} was the glucuronide conjugate of ST [8]. However, M_{26} could not be further studied by MS^n owing to its too low concentration and thus no exact structural assignment could be suggested.

3.2.2 Identification of BR metabolites

23 metabolites of BR, including 17 phase I and six phase II metabolites, were detected in rat urine. Since BR shares two metabolites with ST (M_{12} and M_{15}), which had already been identified above, we will not repeat these here. The structural elucidation and identification for other BR metabolites were as follows.

M_1' and M_2' showed average $[M + H]^+$ at m/z 381.18117, and thus they were tentatively proposed to be demethylation products at C_2 or C_3 [5]. Since M_1' and M_2' had similar MS^2 product ions, we could not propose the exact demethylation sites at this time.

M_3', M_4', and M_5' were observed as average $[M + H]^+$ at m/z 411.19184, suggesting that they were isomers of hydroxylation or oxidation metabolites of BR. Their MS^2 fragment ions of some isomeric metabolites (Supporting Information Fig. S6) were similar with corresponding ST metabolites and were 60 higher than those of ST, which could be used for their differentiation. MS^2 product ions of M_3' at m/z 340.11835, 365.14999, 383.16051, and 393.18130 clearly suggested hydroxylation at C_{22} of the seven-membered ring. Thus, we propose M_3' as 22-hydroxyBR. On the contrary, no characteristic fragments were detected in MS^2 spectrum of M_4'. During the production of ion m/z 280.09729 (loss of the $C_{17–23}$, N_{19} and O_{24} moiety), alternative pathways were available for M_3', but not M_4', to produce m/z 282 and 340 (loss of the nitrogen bridges). The above information implies that M_4' has a hydroxylation substituent at either position C_{13} or C_{14}, but the site could not be exactly determined. M_6' fragmented in a similar way to M_4 and produced the product ions at m/z 393.18127, 367.16565, 324.12357, and 298.10782, which were 60 more than M_4. Therefore, M_6' was

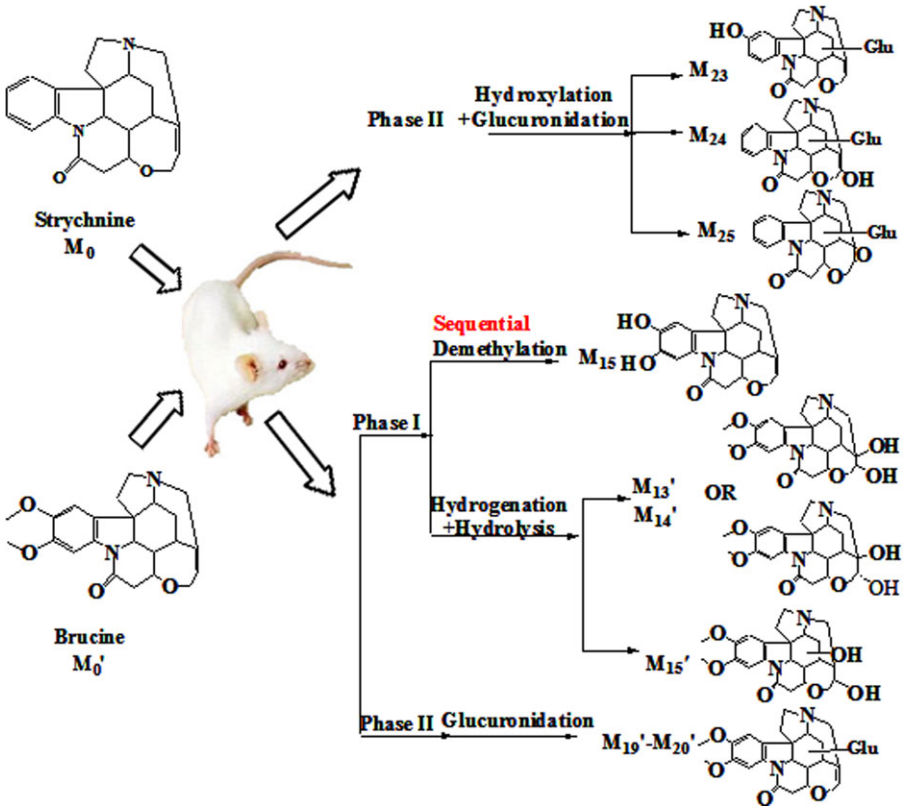

Figure 5. Representative proposed metabolism of ST and BR.

identified as 16-hydroxyBR. Likewise, M_7' produced a base peak at m/z 394.18930 and a minor ion at m/z 379.16580, which were 60 higher than those of M_5. The retention time, accurate mass, and tandem mass spectrum of M_7' were the same as the authentic standard. Thus M_7' was confirmed as BR *N*-oxide. The major MS^2 fragment ions of M_5' were at m/z 320.17078, 304.0976, and 244.06699, corresponding to the loss of $C_3H_9NO_2$, $C_4H_{13}NO_2$, and whole seven-membered ring, respectively, suggesting that the hydroxylation took place at C_{12}. Therefore, M_5' was proposed as 12-hydroxyBR [15].

Metabolites M_8'-M_{12}' showed an average $[M + H]^+$ at m/z 427.18664, 32 higher than BR, suggesting that they were sequential oxidation or hydroxylation metabolites of BR. Their MS^2 spectra all exhibited identical base peaks at m/z 409, suggesting that a hydroxylation occurred on the seven-membered ring or C_{16} position of BR. However, at this time the site could not be exactly proposed.

The average $[M + H]^+$ of metabolites M_{13}'–M_{15}' were at m/z 429.20256, 34 more than m/z 395.19653, preliminarily indicating that all of them were the hydroxylation–hydrolysis products of BR. Cleavage of M_{13}' and M_{14}' were similar to M_8 and M_9, and the MS^2 characteristic product ions (Supporting Information Fig. S7) at m/z 411.19193, 393.18137, 272.12951, 411.25162, 393.22403, and 272.18994 were 60 higher than those of M_8 and M_9. Naturally, they both were identified as 21,22-dihygroxy-22-hydroBR. MS^2 product ions of M_{15}' were similar to the MS^3 product ions of M_{10} (Fig. 3), it was hence proposed as dihydroxy-22-hydroBR.

3.2.2.1 Phase II metabolites of BR

M_{16}', M_{17}' and M_{18}' exhibited an average $[M+H]^+$ at m/z 557.21371, which was 162 more than BR, suggesting that demethylation–glucuronidation reactions had occurred. As they all exhibited MS^2 product ions near m/z 381.18140 (loss of $C_6H_8O_6$), the corresponding MS^3 spectra (Supporting Information Fig. S8) were examined to find detailed structure information. Results showed that their MS^3 spectrum were almost the same, and quite similar to the MS^2 spectrum of M_1' and M_2'. Consequently, they were proposed as the glucuronide conjugate of demethylated BR [5].

The $[M + H]^+$ of M_{19}'–M_{21}' were near m/z 571.22664, 176 more than m/z 395.19653, indicating that they were isomers of the glucuronide conjugate of BR. The MS^2 product ions of M_{19}' and M_{20}' were almost the same, and they both exhibited the predominant MS^2 product ions at m/z 381 (Supporting Information Fig. S9). However, we could not characterize any of their exact sites of glucuronidation based on the limited MS data.

3.3 Metabolism pathways of ST and BR in rats

In an earlier *in vitro* metabolism study, 31 metabolites of ST and BR were identified in rat liver microsomes using LC–HRMS [15]. In our study, 47 metabolites of ST and BR in rat urine were also detected by LC–HRMS. Based on these results, we proposed the possible metabolism pathways of ST and BR in rats and compared that with the *in vitro*

data (Table 2). Results showed that main metabolism pathways of ST and BR proposed in the *in vivo* study were also found in the *in vitro* study. The exceptions had two sources: one was some low-concentration phase-I metabolites, such as hydroxylation–hydrolysis products of ST and sequential demethylation products of BR; the other was the phase-II metabolites, such as glucuronidation products of both. Besides, we confirmed two metabolites with authentic standards. This not only suggested that the *in vivo* metabolism pathways of ST and BR correlated well with *in vitro* ones, but also proved that our *in vivo* studies a represented more realistic picture about the metabolism of SAs in rats.

Most of the other reported metabolites were also identified and metabolism pathways were proposed, such as hydroxylation–hydrolysis ST [24] and demethylation–glucuronidation of BR [5]. Besides, 25 new metabolites of ST and BR formed *in vivo* were identified and four new metabolism pathways were proposed (Fig. 5), including hydroxylation–glucuronidation of ST, sequential demethylation, hydroxylation—hydrolysis, and glucuronidation of BR. These data supplement the *in vivo* metabolism characteristics of SAs in rats, and further support the reliability of our methodology.

4 Concluding remarks

The *in vivo* metabolism of SAs in rats was studied extensively by combination of multistage fragment ions with accurate mass measurements using UHPLC–LTQ-Orbitrap-MS. As a result, 25 *in vivo* metabolites and four *in vivo* metabolism pathways were presented for the first time in our study. This work will clarify more comprehensively the *in vivo* metabolism characteristics of SAs in rats, and moreover will contribute a lot in the field of toxic substances screening and metabolites identification.

The authors have declared no conflict of interest.

5 References

[1] Chen, X. G., Lai, Y. Q., Cai, Z. W., *J. Anal. Toxicol.* 2012, *36*, 171–176.

[2] Philippe, G., Angenot, L., Tits, M., Frédérich, M., *Toxicon* 2004, *44*, 405–416.

[3] Yu, Z., Wu, Z., Gong, F., Wong, R., Liang, C., Zhang, Y., Yu, Y., *J. Sep. Sci.* 2012, *35*, 2773–2780.

[4] Wang, Z., Zhao, J., Xing, J., He, Y., Guo, D., *J. Anal. Toxicol.* 2004, *28*, 141–144.

[5] Tsukamoto, H., Yoshimura, H., Watabe, T., Oguri, K., *Biochem. Pharmacol.* 1964, *13*, 1577–1586.

[6] Oguri, K., Tanimoto, Y., Mishima, M., Yoshimura, H., *Xenobiotica* 1989, *19*, 171–178.

[7] Tanimoto, Y., Ohkuma, T., Oguri, K., Yoshimura, H., *Xenobiotica* 1991, *21*, 395–402.

[8] Guo, J. F., Chen, X. Y., Zhong, D. F., Chin. *J. Pharm. Anal.* 2001, *21*, 167–170.

[9] Hudson, S., Ramsey, J., King, L., Timbers, S., Maynard, S., Dorgan, P. I., Wood, D. M., *J. Anal. Toxicol.* 2010, *34*, 252–260.

[10] Sauvage, F., Picard, N., Saint-Marcoux, F., Gaulier, J., Lachâtre, G., Marquet, P., *J. Sep. Sci.* 2009, *32*, 3074–3083.

[11] Liu, M. Y., Zhao, S. H., Wang, Z. Q., Wang, H. T., Shi, X. W., Lu, Z. M., Xu, H. H., Wang, H. R., Du, Y. F., Zhang, L. T., *J. Sep. Sci.* 2011, *34*, 3200–3207.

[12] Wishart, D. S., *Bioanalysis* 2011, *3*, 1769–1782.

[13] Wong, C. C., Cociorva, D., Venable, J. D., Xu, T., Yates, J. R., *J. Am. Soc. Mass Spectrom.* 2009, *20*, 1405–1414.

[14] Jirasko, R., Holcapek, M., Vrublova, E., Ulrichova, J., Simanek, V., *J. Chromatogr. A.* 2010, *1217*, 4100–4108.

[15] Tian, J. X., Peng, C., Xu, L., Tian, Y., Zhang, Z. J., *Biomed. Chromatogr.* 2013, *27*, 775–783.

[16] Peterman, S. M., Duczak Jr, N., Kalgutkar, A. S., Lame, M. E., Soglia, J. R., *J. Am. Soc. Mass Spectrom.* 2006, *17*, 363–375.

[17] Dunn, W. B., Broadhurst, D., Brown, M., Baker, P. N., Redman, C., Kenny, L. C., Kell, D. B., *J. Chromatogr. B.* 2008, *871*, 288–298.

[18] Liu, T., Du F., Wan, Y., Zhu, F., Xing, J., *J. Mass Spectrom.* 2011, *46*, 725–733.

[19] Shan, Q., Liu, Y. M., He, L. M., Ding, H. Z., Huang, X. H., Yang, F., Li, Y. F., Zeng, Z. L., *J. Chromatogr. B.* 2012, *881–882*, 96–106.

[20] Du, F., Ruan, Q., Zhu, M., Xing, J., *J. Mass Spectrom.* 2013, *48*, 413–422.

[21] Thomas, A., Walpurgis, K., Krug, O., Schänzer, W., Thevis, M., *J. Chromatogr. A* 2012, *1259*, 251–257.

[22] Peterman, S. M., Duczak, N. J., Kalgutkar, A. S., Lame, M. E., Soglia, J. R., *J. Am. Soc. Mass Spectrom.* 2006, *17*, 363–375.

[23] Tanimoto, Y., Ohkuma, T., *J. Pharmacobio-Dyn.* 1990, *13*, 136–141.

[24] Mishima, M., Tanimoto, Y., Oguri, K., Yoshimura, H., *Drug Metab. Dispos.* 1985, *13*, 716–721.

